

Emergence of Orbital Angular Momentum by Inversion Symmetry Breaking and Its Detection by ARPES

Choong H. Kim,¹ Jin-Hong Park,² Jun Won Rhim,³ Beom Young Kim,⁴ Jaejun Yu,¹ Masashi Arita,⁵ Kenya Shimada,⁵ Hirofumi Namatame,⁵ Masaki Taniguchi,⁵ Changyoung Kim,^{4,*} and Jung Hoon Han^{2,†}

¹*Department of Physics and Astronomy, Seoul National University, Seoul 151-742, Korea*

²*Department of Physics and BK21 Physics Research Division, Sungkyunkwan University, Suwon 440-746, Korea*

³*School of Physics, Korea Institute for Advanced Study, Seoul 130-722, Korea*

⁴*Institute of Physics and Applied Physics, Yonsei University, Seoul, Korea*

⁵*Hiroshima Synchrotron Radiation Center, Hiroshima University, Higashi-Hiroshima, Hiroshima 739-0046, Japan*

(Dated: December 18, 2018)

Rashba-split surface band is characterized by a one-to-one correspondence between the electron's momentum \mathbf{k} and its spin orientation. Here we show that a similar correspondence between momentum and orbital angular momentum (OAM) must exist on surface bands once the inversion symmetry is broken. The correspondence is valid even when there is no spin-orbit interaction. Tight-binding and first-principles calculations are presented to support our claim. As a method to detect such OAM-momentum correspondence, we propose the circular dichroism (CD) experiment using the angle-resolved photoemission (ARPES) setup. CD-ARPES experiment performed on Cu surface confirms the existence of chiral OAM. A new concept of "orbital Galvanic effect" is proposed.

PACS numbers:

Electrons in solids are classified by several quantum numbers, including their momentum, spin, and sometimes orbital angular momentum (OAM). In some cases two or more degrees of freedom appear in coupled form as, for instance, in the Rashba phenomena where there exists a one-to-one correspondence between the electron's momentum and its spin[1]. Rashba effects are prominent in certain surface bands[2] or in a bulk insulator[3] lacking the inversion symmetry. In addition to inversion symmetry breaking (ISB), spin-orbit interaction (SOI) is the pre-requisite for the observability of Rashba-related phenomena. The relation of SOI to Rashba splitting has been discussed by several authors in the past[4], and recently by some of the present authors[5].

The implication of ISB on the Rashba splitting is anticipated on symmetry grounds. With the surface normal along the \hat{z} -direction, one can write down a symmetry-allowed Hamiltonian $H_R = \lambda_R \hat{z} \cdot (\mathbf{k} \times \boldsymbol{\sigma})$ in terms of the spin operator $\boldsymbol{\sigma}/2$ and electronic momentum \mathbf{k} . The Rashba energy scale λ_R appearing in H_R is on the order of the electrostatic potential barrier across the surface, multiplied by its width[5]. The chiral spin angular momentum (SAM) structure in momentum space follows as a direct consequence of the Rashba Hamiltonian H_R . Such chiral SAM structure has been thoroughly documented on surfaces of several metallic elements[6, 7] as well as on the surfaces of topological insulators[8] in recent years. Its potential as an effective source of spin current is also being actively investigated[7].

Upon closer inspection, however, one finds that other physical quantities with the same symmetry properties can take the place of $\boldsymbol{\sigma}$ in the Rashba Hamiltonian. It is conceivable, for instance, to replace $\boldsymbol{\sigma}$ by the orbital

angular momentum operator \mathbf{L} in a degenerate orbital system where \mathbf{L} is an active degree of freedom. In the case of materials with strong spin-orbit interaction (SOI), the total angular momentum $\mathbf{J} = \mathbf{L} + (1/2)\boldsymbol{\sigma}$ may be the more appropriate choice[5]. Both scenarios would imply chiral OAM structure in much the same way that chiral SAM follows from the Rashba Hamiltonian. We show that chiral OAM in one-to-one correspondence with the electron's linear momentum is indeed a general consequence of ISB at the surface and should occur on surface bands even for materials with no SOI, placing OAM as the more generic feature of ISB than SAM is.

The above symmetry consideration is further supported by the analysis of a tight-binding (TB) model of two-dimensional monolayer of atoms. For simplicity we will consider an sp -orbital system with three degenerate p -orbitals forming bands. To emphasize the notion of ISB-induced OAM better, we will first study the spinless case to show that OAM can arise without SOI and only later introduce SOI as a perturbation. The latter procedure is shown to recover the usual Rashba spin splitting. It will be shown that the phenomenon of chiral OAM is described by a two-dimensional massive Dirac Hamiltonian.

The tight-binding model of spinless p -orbitals can be constructed in terms of two Slater-Koster parameters V_1 and V_2 for σ - and π -bonding amplitudes, respectively, and a third one, γ , representing the degree of ISB[4]. In real materials, γ arises from the surface-normal electric field which breaks the inversion symmetry. Degeneracy of atomic p -orbital states is assumed in our model, which is justified in simple elements like Cu, Sb and Bi due to their weak crystal field splitting. We will write N for the

number of sites in the lattice, and $|i, p_\lambda\rangle$ for the localized Wannier orbitals ($\lambda = x, y, z$) at the atomic site \mathbf{r}_i . Then the tight-binding Hamiltonian for the triangular lattice (essentially the same result obtains for square lattice) near the Γ -point ($\mathbf{k} = 0$) in the momentum-space basis $|\mathbf{k}, p_\lambda\rangle = N^{-1/2} \sum_i e^{i\mathbf{k}\cdot\mathbf{r}_i} |i, p_\lambda\rangle$ becomes

$$H_{\mathbf{k}} = \begin{pmatrix} \alpha k_x^2 + \beta k_y^2 & (\alpha - \beta)k_x k_y & -i\frac{3}{2}\gamma k_x \\ (\alpha - \beta)k_x k_y & \alpha k_y^2 + \beta k_x^2 & -i\frac{3}{2}\gamma k_y \\ i\frac{3}{2}\gamma k_x & i\frac{3}{2}\gamma k_y & 4(\alpha - \beta) - \frac{3}{2}V_2 k^2 \end{pmatrix}. \quad (1)$$

Here, $\alpha = 3(3V_1 - V_2)/8$, $\beta = 3(V_1 - 3V_2)/8$ and $k^2 = k_x^2 + k_y^2$. The lattice constant is taken to be unity. To diagonalize $H_{\mathbf{k}}$, it is convenient to choose a new set of basis vectors

$$\begin{aligned} |\text{I}, \mathbf{k}\rangle &= (k_y/k)|p_x, \mathbf{k}\rangle - (k_x/k)|p_y, \mathbf{k}\rangle, \\ |\text{II}, \mathbf{k}\rangle &= (k_x/k)|p_x, \mathbf{k}\rangle + (k_y/k)|p_y, \mathbf{k}\rangle, \\ |\text{III}, \mathbf{k}\rangle &= e^{-i\phi_{\mathbf{k}}}|p_z, \mathbf{k}\rangle, \end{aligned} \quad (2)$$

$k = |\mathbf{k}|$, $e^{i\phi_{\mathbf{k}}} = (k_x + ik_y)/k$. The state $|\text{I}, \mathbf{k}\rangle$ remains decoupled at energy $E_{1,\mathbf{k}} = 3V_2 - 3V_1 + 3(V_1 - 3V_2)\mathbf{k}^2/8$, while $|\text{II}, \mathbf{k}\rangle$ and $|\text{III}, \mathbf{k}\rangle$ obey a reduced 2×2 Hamiltonian

$$H_{\text{OAM}} = -4\beta I_{2 \times 2} + M^{-1}\mathbf{k}^2 + \frac{3}{2}\hat{z} \cdot (\gamma\mathbf{k} \times \boldsymbol{\tau} - \Delta\boldsymbol{\tau}^z), \quad (3)$$

with $\Delta = V_1 + V_2$ the bandwidth, $M^{-1} = \begin{pmatrix} \alpha & 0 \\ 0 & -3V_2/2 \end{pmatrix}$ the effective mass tensor, and $\boldsymbol{\tau}$ the pseudo-spin matrix. Eigenstates in the leading order of γ/Δ are

$$\begin{aligned} |2, \mathbf{k}\rangle &\simeq |\text{II}, \mathbf{k}\rangle - \frac{i\gamma(k_x - ik_y)}{2\Delta} |\text{III}, \mathbf{k}\rangle, \\ |3, \mathbf{k}\rangle &\simeq |\text{III}, \mathbf{k}\rangle - \frac{i\gamma(k_x + ik_y)}{2\Delta} |\text{II}, \mathbf{k}\rangle, \end{aligned} \quad (4)$$

with energies $E_{2,\mathbf{k}} \simeq 3(V_2 - V_1) + 3((3V_1 - V_2)/8 - \gamma^2/4\Delta)\mathbf{k}^2$ and $E_{3,\mathbf{k}} \simeq 6V_2 + (3\gamma^2/4\Delta - 3V_2/2)\mathbf{k}^2$. The OAM operator is given by the sum $\mathbf{L} = (1/N) \sum_i \mathbf{L}_i$ where each \mathbf{L}_i acts on the Wannier state $|i, p_\lambda\rangle$ as the usual $L = 1$ angular momentum operator. The two bands obtained above carry nonzero OAM as claimed ($L^+ = L^x + iL^y$):

$$\langle 2, \mathbf{k} | L^+ | 2, \mathbf{k} \rangle = \frac{i\gamma}{\Delta} (k_x + ik_y) = -\langle 3, \mathbf{k} | L^+ | 3, \mathbf{k} \rangle. \quad (5)$$

Both bands possess a chiral pattern of OAM whose strength is proportional to the ISB parameter γ and are opposite between the two bands. OAM for the decoupled state $|\text{I}, \mathbf{k}\rangle$ is vanishing because it consists of p_x and p_y orbitals only ($L_z = \pm 1$) and does not contain p_z ($L_z = 0$). The reduced Hamiltonian (3) satisfies time-reversal invariance. The size of OAM gets reduced linearly with

the momentum $|\mathbf{k}|$ and with the symmetry-breaking parameter γ . By contrast, the magnitude of polarized spin in the Rashba model is independent of the Rashba parameter λ_R .

Incorporating the spin degree of freedom at each atomic site as the Pauli matrix $\boldsymbol{\sigma}_i$, we can examine the influence of the SOI interaction $H_{\text{so}} = (\lambda_{\text{so}}/2) \sum_i \mathbf{L}_i \cdot \boldsymbol{\sigma}_i$ as a perturbation for each band obtained above. The spin-orbit interaction energy λ_{so} is assumed smaller than either the ISB energy γ or the bandwidth Δ . Employing the standard degenerate perturbation theory for the two spin states at a given \mathbf{k} -vector, we find the resulting matrix elements $\langle n, \mathbf{k}, s | H_{\text{so}} | n, \mathbf{k}, s' \rangle$ ($s, s' = \uparrow, \downarrow$) form a 2×2 Rashba-type Hamiltonian matrix

$$\pm \frac{3}{2} \lambda_{\text{so}} \frac{\gamma}{\Delta} \hat{z} \cdot \mathbf{k} \times \boldsymbol{\sigma} \quad (6)$$

for bands $n = 2$ and $n = 3$, respectively. There is no Rashba splitting for band 1 within the degenerate perturbation theory. Combined with the analysis of chiral OAM, we obtain the following hierarchy of chiral angular momenta: First, there is chiral OAM arising from ISB alone. At the next level, when a small SOI is present, each spin-degenerate OAM-carrying band is split into a pair of bands carrying opposite chiral SAMs. Both chiral structures are embodied in Dirac-like effective Hamiltonians, with the energy scale for chiral OAM dominant over that of chiral SAM by the factor $\Delta/\lambda_{\text{so}}$. Chiral OAM, unlike SAM, can be substantial for surfaces consisting of light elements, and its strength controlled by applying an inversion-symmetry-breaking electric field externally.

To ensure that chiral OAM exists in a more realistic calculation, we performed first-principles local-density approximation (LDA) calculation for a Bi single layer forming a triangular lattice. The choice is inspired by Bi being a proto-typical p -orbital band material. An external electric field of $3V/\text{\AA}$ perpendicular to the layer was imposed by hand to mimic the surface potential gradient without having the complication of dealing with the bulk states. The physically more relevant case of Bi layer is also considered[9], with LDA results easily adaptable to the single-layer case discussed below. To emphasize the relevance of ISB we chose to investigate the spin-degenerate by turning off SOI in the LDA calculation. The resulting electronic structure for spinless case consisting of three p -orbital-derived bands is shown in Fig. 1(a). As the external electric field is turned on, a level repulsion between the middle (E_2 in Fig. 1(a)) and the bottom (E_3 in Fig. 1(a)) band occurs as indicated by circles in Fig. 1(a). These two bands exhibit the chiral OAM patterns with the maximum OAM vector $|\langle \mathbf{L} \rangle| \approx 0.96\hbar$ as shown in Fig. 1(c) and 1(d), while the third one, shown in Fig. 1(b), carries much less OAM around the Γ point. The OAM chiralities of the two bands are opposite, in accordance with the previous TB

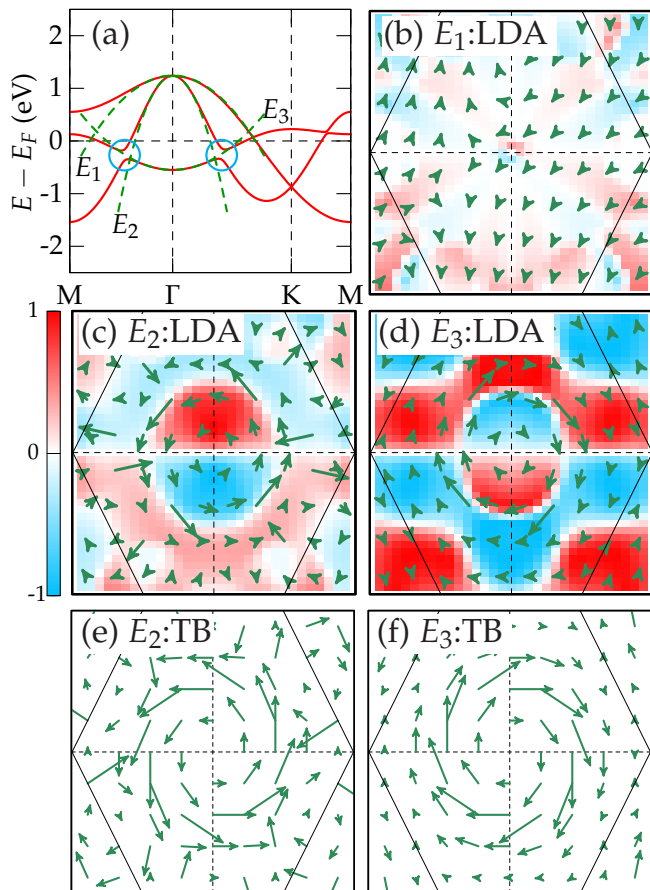


FIG. 1: OAM and CD from first-principles and tight-binding calculations of Bi monolayer without SOI. (a) LDA band structure for Bi monolayer of triangular lattice structure without SOI. Perpendicular electric field of $3\text{V}/\text{\AA}$ was imposed externally. Three dashed curves represent the tight-binding energy dispersions around the Γ point. (b)-(d) OAM vectors (green arrows) and CD signals (color backgrounds) for the three bands from the highest (E_1) to lowest (E_3) energies over the whole Brillouin zone marked by a solid hexagon. Largest OAM has magnitude $\approx 1\hbar$ for bands E_2 and E_3 . Incoming photon direction $\mathbf{k}_{\text{ph}} = +\hat{x}$ is assumed for the CD calculation. (e)-(f) OAM obtained from the tight-binding calculation for two main OAM-carrying bands E_2 and E_3 .

analysis. An excellent fit of the LDA band structure near the Γ point was possible with the TB parameters $V_1 = -0.725$ eV, $V_2 = -0.11$ eV and $\gamma = 0.2623$ eV (Fig. 1(a)). The good fit by the TB model is a testament to the negligible crystal field effect in the elemental Bi. OAM values obtained by the TB analysis are also in excellent quantitative accord with the LDA results as can be seen by comparing Fig. 1(c)-(d) (LDA) to Fig. 1(e)-(f) (TB). The OAM magnitude is seen to decrease continuously upon approaching the Γ point in the LDA calculation (Fig. 1(c) and 1(d)) as predicted by the TB calculation, Eq. (5).

Having established theoretically the existence of chiral OAM in inversion-asymmetric bands by a num-

ber of methods, we turn to the question of its detection. Spin- and angle-resolved photoemission spectroscopy (SARPES) has served to identify the chiral spin structure of the surface bands in the past[6, 7]. A similar chiral structure for OAM as demonstrated here cannot, however, be detected by the same probe since chiral OAM exists even when SOI is very weak and spin degeneracy is nearly perfect. Circular dichroism (CD) refers to phenomena in which the physical response of a system to probing light depends systematically on the light polarization being left-circularly-polarized (LCP) or right-circularly-polarized (RCP). In ARPES experiment, in particular, incident lights of opposite helicities (RCP vs. LCP) might give rise to different scattering intensities of photo-electrons. It can be shown, in fact, that such difference is a consequence of finite OAM polarization in \mathbf{k} -space and can be used to detect its existence.

One can formally define the CD-ARPES signal $D(\mathbf{k})$ as

$$D(\mathbf{k}) = \frac{\sum_{\sigma} (I_{\sigma}^{\text{RCP}}(\mathbf{k}) - I_{\sigma}^{\text{LCP}}(\mathbf{k}))}{\sum_{\sigma} (I_{\sigma}^{\text{RCP}}(\mathbf{k}) + I_{\sigma}^{\text{LCP}}(\mathbf{k}))}. \quad (7)$$

Here $I_{\sigma}(\mathbf{k})$ refers to the probability of scattering from an initial occupied state at momentum \mathbf{k} to a final photo-electron state of spin orientation σ . Since we have spin-integrated ARPES in mind, the final-state spin is summed. Coupling to electromagnetic fields gives rise to a perturbed Hamiltonian $H_1 \sim \mathbf{p} \cdot \mathbf{A}$ (\mathbf{p} =momentum operator, \mathbf{A} =vector potential). The transition amplitude from the initial state $|I\rangle$ to a final state $|F\rangle$ is proportional to $\langle F|H_1|I\rangle \sim \langle F|\mathbf{r} \cdot \mathbf{A}|I\rangle$, according to standard theory. Taking a plane-wave form for the final state wave function $\psi_F(\mathbf{r}) = e^{i\mathbf{k}_F \cdot \mathbf{r}}$, where \mathbf{k}_F is the wave vector of the final-state photo-electron, and using the initial state wave function obtained from LDA, we can calculate the transition probability for RCP (\mathbf{A}) and LCP (\mathbf{A}^*) incoming lights to get $D(\mathbf{k})$. The in-plane component of \mathbf{k}_F matches the momentum of band electrons (higher-order Umklapp processes are neglected), while the normal component k_F^z can be deduced from energy conservation.

The incident photon direction \hat{k}_{ph} is chosen with its in-plane component along $+\hat{x}$ axis in calculating $D(\mathbf{k})$ for Bi monolayer band structure. The results are color-coded and superimposed on the OAM patterns in Fig. 1(b)-(d). In the case of Bi monolayer the CD intensity proved largely insensitive to the choice of k_F^z value, so we used $k_F^z = 0$ for the displayed result. One can make sense of the CD color patterns from a simple angular momentum conservation argument when \mathbf{k} is close to the Γ point. Defining the projection of the electron angular momentum operator \mathbf{L} onto the photon direction as $\hat{k}_{\text{ph}} \cdot \mathbf{L}$, incident RCP light would increase it by $+\hbar$ whereas LCP light reduces it by \hbar . Therefore, loosely speaking, initial states with $\langle \mathbf{L} \rangle \propto -\hat{x}$ ($l=-1$) is coupled to $l = 0$

($l = -2$) channel of the final state by the RCP (LCP) light. Expansion of the final plane-wave state in terms of spherical harmonics produces a larger weight for $l = 0$ than $l = -2$, thus $D(\mathbf{k}) > 0$ for such an initial state. Following such consideration leads to the result $D(\mathbf{k}) \propto \hat{k}_{\text{ph}} \cdot \langle \mathbf{k} | \mathbf{L} | \mathbf{k} \rangle$.

In Fig. 1(c)-(d), one finds that such elementary consideration to be indeed in accord with the CD patterns near the Γ point. Far from it, though, the color pattern is no longer consistent with it and even gives out the opposite sign, implying that effects besides the conservation rule play a crucial role in determining the overall sign of $D(\mathbf{k})$. In principle, however, all such effects are captured in the LDA calculation and should be compatible with ARPES experiment. We emphasize that CD signal vanishes where OAM disappears, leaving little doubt that the measurement of CD is a direct indicator of local OAM in momentum space. On the other hand, the existence of spin polarization in the band will not be captured by the proposed method even when it is prominent.

Finally, we performed CD-ARPES experiment on Cu surface with a view to confirm the existence of chiral OAM on a realistic material with a small SOI. Because SOI is very small in Cu, it can be safely said that chiral OAM structure is, without question, due to the ISB mechanism proposed here. The calculated band structure of 30 Cu(111) layers is shown in Fig. 2(a). Two surface-derived bands are identified as red curves. In the case of Cu calculation the inversion symmetry-breaking electric field is generated spontaneously through self-consistent electronic structure calculation, and not imposed externally as in the Bi monolayer case. Despite these differences we found a clear, chiral OAM pattern around the Γ point as shown in Fig. 2(b). Even though the make-up of the surface bands receive substantial contributions from both p - and d -orbitals, OAM arises predominantly from the d -orbital components. Using Eq. (7) we can also calculate $D(\mathbf{k})$ for Cu. Contrary to the model Bi calculation, $D(\mathbf{k})$ varies significantly with the choice of the final-state momentum k_F^z . For Fig. 2(b) we used $k_F^z = 2.27\text{\AA}^{-1}$ consistent with the photo-electron energy in the actual experiment described in the next paragraph. The sign of $D(\mathbf{k})$ is opposite to the anticipation from the angular momentum conservation rule near the Γ point. It agrees, however, with the following dichroism experiment performed on Cu surface.

The single, sharp experimental Cu(111) surface band shown in Fig. 2(c) actually consists of two surface bands with opposite spins as found in LDA calculation, unresolved because of the small energy spacing between them. We take the ARPES data twice, one with RCP and the second with LCP lights, and obtain $D(\mathbf{k})$ according to Eq. (7). The results, plotted in Fig. 2(d), cover the small occupied region in Brillouin zone with the Fermi momentum $\approx 0.2\text{\AA}^{-1}$. The CD-ARPES experiment shows pronounced CD behavior that reaches a maximum value

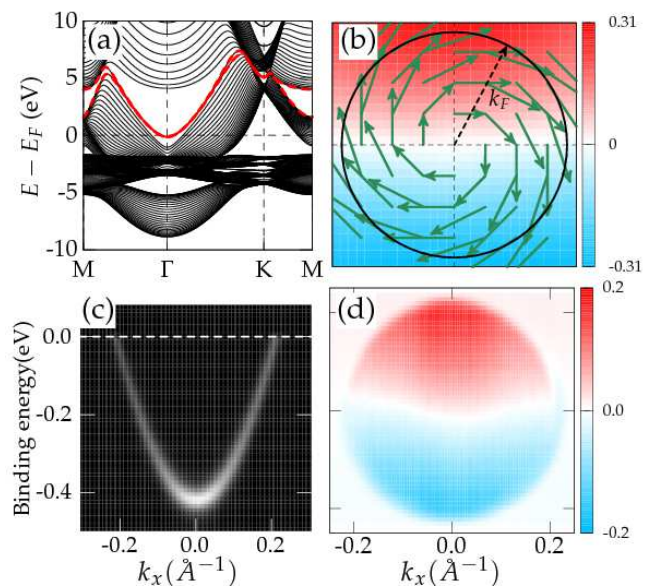


FIG. 2: OAM and CD of Cu surface band. (a) First-principles electronic band structure of Cu(111) 30-layer slab. Red dashed lines indicate the two surface bands. (b) Calculated OAM and CD (assuming the in-plane incident photon direction $\hat{\mathbf{k}}_{\text{ph}} \propto +\hat{x}$) corresponding to outer energy surface bands. Inner surface band shows basically the same OAM and CD patterns. Maximum OAM vector is $\sim 0.07\hbar$. (c) ARPES-measured surface band of Cu along $k_y = 0$. (d) Measured CD-ARPES result $D(\mathbf{k})$. Incident photon direction has in-plane component along $+\hat{x}$. The momentum window in Fig. (b) matches that of Fig. (d).

of $\approx 20\%$ at the Fermi surface, where the OAM is also expected to be the largest. Most importantly, the sign of CD matches that in the LDA calculation, which is a highly non-trivial result given the reversal of the CD sign discussed earlier. The calculated $D(\mathbf{k})$ varies between -0.3 and +0.3, somewhat greater than the 20% variation found experimentally. Thermal effects in the experiment may have contributed to the smearing of CD signal.

Our prediction, and its observation on Cu surface, of chiral OAM is a direct analogue of the well-known chiral SAM from Rashba-split surface bands. Likewise, much of the physical consequences of chiral SAM is expected to have orbital analogues. For instance, spin polarization can drive electrical current through spin-momentum locking in a phenomenon known as the spin Galvanic effect[10]. Its inverse, the spontaneous spin polarization in the current-carrying state of Rashba-split bands, was proposed theoretically by Edelstein[11] and confirmed experimentally in recent years[12]. Having identified OAM as the more fundamental physical quantity associated with ISB, we propose that both these spin-related effects must have orbital analogues.

This work is supported by Mid-career Researcher Program No. 2011-0015631 (JHH), the KICOS through Grant No. K20602000008 (CK), and R17-2008-033-

01000-0 (JY). We acknowledge fruitful conversations with Seung Ryong Park.

* Electronic address: changyoung@yonsei.ac.kr

† Electronic address: hanjh@skku.edu

- [1] Y. A. Bychkov and E. I. Rashba, JETP Lett. **39**, 78 (1984).
- [2] G. Bihlmayer, Yu. M. Koroteev, P. M. Echenique, E. V. Chulkov and S. Blügel, Surf. Sci. **600**, 3888 (2006).
- [3] K. Ishizaka *et al.* Nature Mat. **10**, 521 (2011).
- [4] L. Petersen and P. Hedegård, Surf. Sci. **459**, 49 (2000).
- [5] S. R. Park, C. H. Kim, J. Yu, J. H. Han and C. Kim, Phys. Rev. Lett. **107**, 156803 (2011), and references therein.
- [6] J. H. Dil, J. Phys. Condens. Matter **21**, 403001 (2009).
- [7] A. Kimura *et al.* Phys. Rev. Lett. **105**, 076804 (2010).
- [8] M. Z. Hasan and C. L. Kane, Rev. Mod. Phys. **82**, 3045 (2010).
- [9] Y. Liu and R. E. Allen, Phys. Rev. B **52**, 1566 (1995).
- [10] S. D. Ganichev *et al.* Nature **417**, 153 (2002).
- [11] V. M. Edelstein, Solid State Commun. **73**, 233 (1990).
- [12] A. Chernyshov, M. Overby, X. Liu, J. K. Furdyna, Y. Lyanda-Geller and L. P. Rokhinson, Nature Phys. **5**, 656 (2009).